Optica Applicata, Vol. XLVI, No. 2, 2016
DOI: 10.5277/oa160207

Material parameters of antimonides and amorphous materials for modelling the mid-infrared lasers

ŁUKASZ PISKORSKI*, ROBERT P. SARZAŁA

Photonics Group, Institute of Physics, Lodz University of Technology,
Wólczańska 219, 90-924 Łódź, Poland

*Corresponding author: lukasz.piskorski@p.lodz.pl

The proper modelling of semiconductor device operation with full complexity of many interrelated physical phenomena taking place within its volume is possible only when the material parameters which appear in each part of the self-consistent model are known. Therefore, it is necessary to include in calculations the material composition, temperature, carrier concentration, and wavelength dependences in electrical, thermal, recombination and optical models. In this work we present a complete set of material parameters which we obtained basing mostly on the experimental data found in several dozen publications. To refine the number of equations, we restrict the material list to those which are typically used in edge-emitting lasers and vertical-cavity surface-emitting lasers designed for mid-infrared emission.

Keywords: material parameters, computer simulation, mid-infrared devices, GaSb-based lasers.

1. Introduction

To perform the comprehensive simulation of the operation of a semiconductor device, it is necessary to make use of the complex self-consistent numerical model which is composed of four interrelated parts [1]:

1. The electrical model characterizing both the current spreading (including carrier diffusion) between the top and the bottom contacts, the injection of carriers of both kinds into the active region and the over-barrier leakage of carriers from the active region;
2. The thermal model characterizing generation of a heat flux (non-radiative recombination, reabsorption of spontaneous radiation as well as volume and barrier Joule heating), its spreading within the device from heat sources towards the heat sink and within the heat sink;
3. The gain model furnishing information about the optical gain process within the active regions;
4. The optical model describing, for successive cavity modes, their lasing thresholds, wavelength, intensity profiles within the laser cavity and absorption.

In this theoretical approach, all important, usually nonlinear, interactions between electrical, thermal, recombination and optical phenomena must be taken into account with the aid of the self-consistent approach including [2]: *i*) thermal focusing, *i.e.*, the temperature dependence of refractive indices; *ii*) self-focusing, *i.e.*, the carrier-concentration dependence of refractive indices; *iii*) gain-induced wave-guiding, *i.e.*, the temperature, carrier-concentration and wavelength dependences of the extinction coefficient; *iv*) temperature dependence of thermal conductivities; *v*) temperature and carrier-concentration dependences of electrical conductivities; *vi*) temperature, carrier-concentration and wavelength dependences of optical gain and absorption coefficients; *vii*) temperature and carrier-concentration dependences of the energy gaps.

In the next section we present a complete set of material parameters which we obtained basing mostly on the experimental data found in more than forty publications. In the case of formulas already given in the literature we give only the reference to the article. We restrict the material list to materials which are used in edge-emitting lasers [3] and vertical-cavity surface-emitting lasers [4] designed for mid-infrared emission: Te- and Si-doped GaSb, Te-doped AlAsSb lattice-matched to GaSb, heavily Si-doped InAsSb lattice matched to GaSb, Te-and Si-doped AlGaAsSb with low both Al and As contents, unintentionally doped GaInAsSb quantum wells with GaSb barriers, and two amorphous materials α-Si and SiO_2 which form dielectric mirrors in surface-emitting lasers (SiO_2 can be also deposited as a passivation layer).

2. Material parameters

2.1. Electrical conductivities, mobilities, and free carrier concentrations

Electrical conductivities of the *n*- and *p*-type semiconductor materials can be calculated from the following equations given in [5]:

$$\sigma_n(n, T) = en(N_D, T)\mu_n(n, T) \tag{1}$$

$$\sigma_p(p, T) = ep(N_A, T)\mu_p(p, T) \tag{2}$$

where e is the electron charge, n and p are the free electron and hole concentrations, T is the temperature, N_D and N_A are concentrations of donors and acceptors, and μ_n and μ_p are the electron and hole mobilities.

For temperature dependence of free carrier concentrations we suggest the relations of the following forms:

$$n(N_D, T) = n_{300\,\mathrm{K}}(N_D)\left(\frac{T}{300}\right)^{\delta_n(N_D)} \tag{3}$$

$$p(N_A, T) = p_{300\,\mathrm{K}}(N_A)\left(\frac{T}{300}\right)^{\delta_p(N_A)} \tag{4}$$

where parameters δ_n and δ_p depend only on doping concentrations.

In the case of temperature dependences of carrier mobilities, similar relations can be used [6]:

$$\mu_n(n, T) = \mu_{300\,\mathrm{K}}(n)\left(\frac{300}{T}\right)^{\gamma_n(N_D)} \tag{5}$$

$$\mu_p(p, T) = \mu_{300\,\mathrm{K}}(p)\left(\frac{300}{T}\right)^{\gamma_p(N_A)} \tag{6}$$

where parameters γ_n and γ_p depend only on doping concentrations.

In this section both doping and free carrier concentrations are given in cm^{-3}, carrier mobilities in $\mathrm{cm}^2/\mathrm{Vs}$, and temperatures in K.

Using the existing experimental data [7, 8], we obtain the following expressions for the free carrier concentrations in Te-doped *n*-GaSb and Si-doped *p*-GaSb:

$$n_{\mathrm{GaSb},\,300\,\mathrm{K}}(N_D) = \begin{cases} N_D & \text{for} \quad N_D \le 10^{18}\ \mathrm{cm}^{-3} \\ 10^{0.383027N_L^3 - 22.1278N_L^2 + 425.212N_L - 2700.2222} & \text{for} \quad N_D > 10^{18}\ \mathrm{cm}^{-3} \end{cases} \tag{7}$$

$$p_{\mathrm{GaSb},\,300\,\mathrm{K}}(N_A) = \begin{cases} N_A & \text{for} \quad N_A \le 2.36 \times 10^{17}\ \mathrm{cm}^{-3} \\ [-0.0731 \times \log(N_A) + 2.27]N_A & \text{for} \quad N_A > 2.36 \times 10^{17}\ \mathrm{cm}^{-3} \end{cases} \tag{8}$$

where $N_L = \log(N_D)$. Basing on experimental data given in [9, 10] we assume that parameters δ_n and δ_p for Te- and Si-doped GaSb can be written as:

$$\delta_{n,\,\mathrm{GaSb}}(N_D) = 0.4506 \times \log[n_{\mathrm{GaSb},\,300\,\mathrm{K}}(N_D)] - 7.95 \tag{9}$$

$$\delta_{p,\,\mathrm{GaSb}}(N_A) = \begin{cases} p_{\mathrm{GaSb},\,300\,\mathrm{K}}(N_A) \times 10^{17} & \text{for} \quad p_{\mathrm{GaSb},\,300\,\mathrm{K}} \le 6.4 \times 10^{17}\ \mathrm{cm}^{-3} \\ 0.088 & \text{for} \quad p_{\mathrm{GaSb},\,300\,\mathrm{K}} > 6.4 \times 10^{17}\ \mathrm{cm}^{-3} \end{cases} \tag{10}$$

Using the existing experimental data [9, 11–16], we obtained the following expressions for the carrier mobilities in Te- and Si-doped GaSb:

$$\mu_{n,\,\mathrm{GaSb},\,300\,\mathrm{K}}(n) = 550 + \frac{5750}{1 + \left(\dfrac{n}{2 \times 10^{17}}\right)^{0.786}} \tag{11}$$

$$\mu_{p,\,\mathrm{GaSb},\,300\,\mathrm{K}}(p) = 95 + \frac{470}{1 + \left(\dfrac{p}{4 \times 10^{18}}\right)^{0.85}} \tag{12}$$

Taking into consideration the experimental data given in [9, 16], we assume that parameters γ_n and γ_p for Te- and Si-doped GaSb are equal to 1 and 1.2, respectively.

On the basis of [12] we assume that in the case of *n*-AlAsSb with high Sb content, the formula (7) can also be used. Moreover, basing on results presented in [17], we assume no temperature influence on carrier concentration in this material.

For *n*-type AlAsSb we use the following relation to calculate the electron mobility at 300 K:

$$\frac{1}{\mu_{n,\,\mathrm{AlAsSb},\,300\,\mathrm{K}}(n)} = \frac{x}{\mu_{n,\,\mathrm{AlAs},\,300\,\mathrm{K}}(n)} + \frac{1-x}{\mu_{n,\,\mathrm{AlSb},\,300\,\mathrm{K}}(n)} + \eta_n x(1-x) \tag{13}$$

where x is the As content. Using the existing experimental data [17,18], we obtained the following expression for the carrier mobilities in *n*-doped AlAs and AlSb:

$$\mu_{n,\,\mathrm{AlAs},\,300\,\mathrm{K}}(n) = 30 + \frac{280}{1 + \left(\dfrac{n}{8\times 10^{17}}\right)^2} \tag{14}$$

$$\mu_{n,\,\mathrm{AlSb},\,300\,\mathrm{K}}(n) = 30 + \frac{170}{1 + \left(\dfrac{n}{4\times 10^{17}}\right)^{3.25}} \tag{15}$$

Taking into consideration the results presented in [19], we assume that $\eta_n = -0.0093$. For Te-doped AlAsSb we suggest $\gamma_n = 1.8$ taken from [20].

Due to the lack of experimental data, we assume that in the case of AlGaAsSb with low both As and Al content Eqs. (7)–(10) can be used. For *n*-type AlGaAsSb with very low As content doped with Te we recommend the following relation to calculate the electron mobility at 300 K:

$$\frac{1}{\mu_{n,\,\mathrm{AlGaAsSb},\,300\,\mathrm{K}}(n)} = \frac{x}{\mu_{n,\,\mathrm{AlSb},\,300\,\mathrm{K}}(n)} + \frac{1-x}{\mu_{n,\,\mathrm{GaSb},\,300\,\mathrm{K}}(n)} + \eta_n x(1-x) \tag{16}$$

where x is the Al content. On the basis of [21] we assume that $\eta_n = 0.0096$. In the absence of experimental data we assume that γ for Te-doped AlGaAsSb is the same as for Te-doped GaSb.

Similarly, to calculate the mobility for *p*-type AlGaAsSb doped with Si with low both As and Al contents, the following formula can be used:

$$\frac{1}{\mu_{p,\,\mathrm{AlGaAsSb},\,300\,\mathrm{K}}(p)} = \frac{x}{\mu_{p,\,\mathrm{AlSb},\,300\,\mathrm{K}}(p)} + \frac{1-x}{\mu_{p,\,\mathrm{GaSb},\,300\,\mathrm{K}}(p)} + \eta_p x(1-x) \tag{17}$$

where x is the Al content. With the use of experimental data found in [22], we obtained the following expression for the carrier mobility in Si-doped AlSb:

$$\mu_{p,\,\mathrm{AlSb},\,300\,\mathrm{K}}(p) = 30 + \frac{270}{1 + \left(\dfrac{p}{3\times 10^{17}}\right)^{1.54}} \tag{18}$$

On the basis of [21] we assume that $\eta_p = 0.0006$.

No experimental data have been reported for temperature dependence of the mobility in p-doped AlGaAsSb. Therefore, for this material, we suggest using the same value of γ_p as for Si-doped GaSb.

For InAsSb with high As content we recommend using the following relation to calculate the electron concentration:

$$n_{\mathrm{InAsSb},\,300\,\mathrm{K}}(N_D) = \begin{cases} N_D & \text{for} \quad N_D \le 10^{19}\ \mathrm{cm}^{-3} \\ 10^{-0.259963 N_L^2 + 10.9705 N_L - 95.5924} & \text{for} \quad N_D > 10^{19}\ \mathrm{cm}^{-3} \end{cases} \tag{19}$$

which we assumed basing on experimental data given in [23] for n-type InAs. Basing on experimental data given in [24], we assume that parameter δ for Si-doped InAsSb can be written as

$$\delta_{n,\,\mathrm{InAsSb}}(N_D) = -0.00332 \times \log[n_{\mathrm{InAsSb},\,300\,\mathrm{K}}(N_D)] + 0.26 \tag{20}$$

Using the existing experimental data [25], we obtained the following expression for the carrier mobility in Si-doped InAsSb with low Sb content:

$$\mu_{n,\,\mathrm{InAsSb},\,300\,\mathrm{K}}(n) = 450 + \frac{11550}{1 + \left(\dfrac{n}{2\times 10^{18}}\right)^{0.80}} \tag{21}$$

Taking into consideration the experimental data given in [6], we assume that parameter $\gamma_n = 1.7$ for Si-doped InAsSb.

For amorphous materials we suggest electrical conductivities equal to 0.1 $\Omega^{-1}\mathrm{m}^{-1}$ for α-Si [26], to 1×10^{-13} $\Omega^{-1}\mathrm{m}^{-1}$ for SiO_2 [27].

The room-temperature (RT) values of the recombination, namely the monomolecular coefficient A, the bimolecular coefficient B and the Auger coefficient C in the active region with GaInAsSb quantum wells, are assumed on the basis of reported experimental data: $A_{300\mathrm{K}} = 2\times10^{-7}$ s^{-1} [28], $B_{300\mathrm{K}} = 1\times10^{-10}$ cm^3/s [29, 30], $C_{300\mathrm{K}} = 1.05\times10^{-23}\exp(-20.08/E_g)$ cm^6/s [31]. In the case of ambipolar diffusion coefficient we suggest using $D_{300\mathrm{K}} = 10$ cm^2/s which is the same value which we used in computer simulation of mid-infrared laser described in [1]. The temperature dependences of the

recombination coefficients can be written as [32]: $A(T) = A_{300\,\mathrm{K}}(T/300)$, $B(T) = B_{300\,\mathrm{K}}(300/T)^{1.5}$, $C(T) = C_{300\,\mathrm{K}}(T/300)$, and $D(T) = D_{300\,\mathrm{K}}(T/300)$.

2.2. Thermal conductivities

In this section, thermal conductivities are given in W/mK.

Thermal conductivity for GaSb is assumed to be expressed by the following relation [33]:

$$k_{\mathrm{GaSb}}(T) = 36\left(\frac{300\,\mathrm{K}}{T}\right)^{1.35} \tag{22}$$

Thermal conductivities for AlAsSb, InAsSb, AlGaAsSb and GaInAsSb can be obtained from thermal resistivities for binaries (see Table 1) using the following interpolation formulas and bowing parameters taken from [33]:

$$k_{ABC}(x) = \frac{1}{r_{ABC}(x)} = \frac{1}{xr_{AC} + (1-x)r_{BC} + x(1-x)C_{AB}} \tag{23}$$

$$k_{ABCD}(x,y) = \frac{1}{r_{ABCD}(x,y)} = \frac{1}{r_1 + r_2} \tag{24}$$

where: $r_1 = xyr_{AC} + x(1-y)r_{AD} + (1-x)yr_{BC} + (1-x)(1-y)r_{BD}$ and $r_2 = x(1-x)C_{AB} + y(1-y)C_{CD}$.

For α-Si we suggest the following expression:

$$k_{\alpha\text{-Si}}(T) = 20.48\left(\frac{T}{300}\right)^{0.824} + 1.1\left(\frac{T}{300}\right)^{2} - 18.9\left(\frac{T}{300}\right) - 1.07 \tag{25}$$

for temperatures from 77 to 400 K range and:

$$k_{\alpha\text{-Si}}(T) = 2.5215 \times 10^{-4} \times T + 1.5432 \tag{26}$$

for temperatures higher than 400 K. The above temperature dependences we obtained by fitting the data found in [34].

Analogously, the thermal conductivity for SiO_2 is determined from the following formula:

$$k_{\mathrm{SiO_2}}(T) = 0.303\left(\frac{T}{300}\right)^{0.0194} - 1.9 \times 10^{-4} \times \left(\frac{T}{300}\right)^{2} - 0.2899 \tag{27}$$

which we derived for 77–750 K range using the data taken from [35].

2.3. Gain parameters

In order to calculate the gain in the active region, it is necessary to calculate the following parameters for quantum well, barrier and claddings: energy gaps, split-off en-

T a b l e 1. RT thermal conductivities $k_{300\,K}$ and resistivities $r_{300\,K}$ of binary materials together with parameter n describing the temperature dependences of thermal conductivity $k(T) = k_{300\,K}(300/T)^n$. Bowing parameters necessary to obtain the thermal conductivity for ternaries and quaternaries have also been listed.

Parameter	AlAs	AlSb	GaAs	GaSb	InAs	InSb
$k_{300\,K}$ [W/(m·K)]	91	57	45	36	30	17.5
$r_{300\,K}$ [m·K/W]	0.0110	0.0175	0.0222	0.0278	0.033	0.0571
n	1.37	1.42	1.28	1.35	1.73	1.60
Bowing parameter [m·K/W]	C_{AlGa}	C_{GaIn}	C_{AsSb}			
	0.32	0.72	0.91			

T a b l e 2. Gain parameters for binary materials: a_{lc} – lattice constant, E_{g_0} – energy gap at 0 K, α, β – Varshni parameters, Δ_{so} – split-off energy, m_e, m_{hh}, m_{lh} – effective masses of electrons, heavy- and light-holes, E_{v_0} – valence band edge for unstrained material, a_c, a_v, b – deformation potentials, c_{11}, c_{12} – elastic constants.

Parameter	GaAs	AlAs	InAs	GaSb	AlSb	InSb
a_{lc} [Å]	5.65325	5.6611	6.0583	6.0959	6.1355	6.4794
da_{lc}/dT [Å/K]	3.88×10^{-5}	2.90×10^{-5}	2.74×10^{-5}	4.72×10^{-5}	2.60×10^{-5}	3.48×10^{-5}
E_{g_0} [eV]	1.519	3.099	0.417	0.812	2.386	0.235
α [meV/K]	0.5405	0.885	0.276	0.417	0.42	0.32
β [K]	204	530	93	140	140	170
Δ_{so} [eV]	0.341	0.28	0.39	0.76	0.676	0.81
m_e [m_0]	0.067	0.124	0.024	0.039	0.14	0.013
m_{hh} [m_0]	0.33	0.51	0.26	0.22	0.47	0.24
m_{lh} [m_0]	0.090	0.18	0.027	0.045	0.16	0.015
E_{v_0} [eV]	–0.80	–1.33	–0.59	–0.03	–0.41	0
a_c [eV]	–7.17	–5.64	–5.08	–7.5	–4.5	–6.94
a_v [eV]	1.16	2.47	1.00	0.8	1.4	0.36
b [eV]	–2.0	–2.3	–1.8	–2.0	–1.35	–2.0
c_{11} [GPa]	122.1	125.0	83.29	88.42	87.69	68.47
c_{12} [GPa]	56.6	53.4	45.26	40.26	43.41	37.35

T a b l e 3. Nonzero bowing parameters of ternary and quaternary compounds: E_g – energy gap, Δ_{so} – split-off energy, m_e, m_{lh} – effective masses of electrons and light-holes, E_{v_0} – valence band edge for unstrained material, a_c – conduction band deformation potential.

Bowing parameter for	GaInAs	GaInSb	GaAsSb	InAsSb	AlAsSb
E_g [eV]	0.477	0.415	1.43	0.67	0.8
Δ_{so} [eV]	0.15	0.1	0.6	1.2	0.15
m_e [m_0]	0.008	0.010	0.014	0.027	–
m_{lh} [m_0]	–	0.015	–	–	–
E_{v_0} [eV]	–0.38	–	–1.06	–	–1.71
a_c [eV]	2.61	–	–	–	–
Bowing parameter for	AlGaAs	AlGaSb	GaInAsSb	AlGaAsSb	
E_g [eV]	$-0.127 + 1.31x_{Al}$	$-0.044 + 1.22x_{Al}$	0.75	0.812	
Δ_{so} [eV]	–	0.3	–	–	

ergies, effective masses, deformation potentials, and elastic constants. All of them can be found in [33, 36] for binary materials (Table 2). For ternaries $A_xB_{1-x}C$ and quaternaries $A_xB_{1-x}C_yD_{1-y}$ the above parameters can be obtained with the use of interpolation schemes [37]:

$$T_{ABC}(x) = xB_{AC} + (1-x)B_{BC} - x(1-x)C \tag{28}$$

$$\begin{aligned} Q_{ABCD}(x,y) = {} & (1-x)yB_{BC} + xyB_{AC} + x(1-y)B_{AD} + (1-x)(1-y)B_{BD} + \\ & - x(1-x)yC_{ABC} - x(1-x)(1-y)C_{ABD} - xy(1-y)C_{ACD} + \\ & - (1-x)y(1-y)C_{BCD} - x(1-x)y(1-y)C_{ABCD} \end{aligned} \tag{29}$$

where C is the bowing coefficient (see Table 3).

2.4. Refractive indices and absorption coefficients

In this section, absorption coefficients are given in cm^{-1}.

By fitting the experimental data found in [38] and [39], we obtained the following expression for the RT refractive index in undoped GaSb:

$$n_{R,\,\mathrm{GaSb},\,300\,\mathrm{K}}(E) = 0.502E^3 - 1.216E^2 + 1.339E + 3.419 \tag{30}$$

where E stands for the photon energy given in eV. For the doped material the following corrections to the RT value of refractive index should be added, which we derived from the results presented in [40]: $dn_R/dn = -2.9\times10^{-20}$ cm^3, $dn_R/dp = -7.4\times10^{-21}$ cm^3. Temperature dependence of the refractive index of GaSb is given in [6]: $(1/n_R)(dn_R/dT) = 8.2\times10^{-5}$ K^{-1}.

In GaSb, the absorption coefficient, the wavelength and carrier concentration dependence can be described as:

$$\alpha_{n\text{-GaSb, 300 K}}(\lambda, n) = 10^{24}\exp(-\lambda/33) + 1.7\times 10^{-24} n\lambda^{1.95} + \left(20\sqrt{n/10^{18}}\right)^{1.05} \tag{31}$$

where λ is in nm. The above relation we assumed basing on the results presented in [41]. For *p*-type GaSb an analogous relation can be used:

$$\alpha_{p\text{-GaSb, 300 K}}(\lambda, p) = 10^{24}\exp(-\lambda/33) + 2\times 10^{-24} p\lambda^{2} + \left(20\sqrt{p/10^{18}}\right)^{1.05} \tag{32}$$

in which we introduce the corrections in respect to Eq. (31) basing on the data found in [42, 43]. In the absence of experimental data for optical parameters for *n*-AlGaAsSb and *p*-AlGaAsSb with low both Al and As contents, we assume that the relations from (30) to (32) can also be used.

To calculate the refractive index for *n*-AlAsSb, the formula found in [44] can be used, for which we suggest to introduce the following temperature dependence of refractive index [6]: $(1/n_R)(\mathrm{d}n_R/\mathrm{d}T) = [4.6\times 10^{-5}x + 1.19\times 10^{-5}(1-x)]$ K^{-1}, where x is the Al content. To calculate the absorption coefficient for AlAsSb lattice matched to GaSb, we propose the same relation as it is given for *n*-AlSb in [42]: $\alpha = 1.9\times 10^{-24} n\lambda^{2}$.

The refractive index for InAsSb lattice matched to GaSb can be obtained with the use of interpolation of its values for InAs and $InAs_{0.8}Sb_{0.2}$ which we derived from theoretical results presented in [40]:

$$n_{R,\ \mathrm{InAsSb,\ 300\ K}}(\lambda) = 0.01525\lambda^{1.783} + 3.561 \tag{33}$$

$$n_{R,\ \mathrm{InAs,\ 300\ K}}(\lambda) = 0.01525\lambda^{1.783} + 3.561 \tag{34}$$

where λ is given in μm. Free carrier concentration influence on refractive index in InAsSb can be introduced by adding the following term:

$$\Delta n_{R,\ \mathrm{InAsSb,\ 300\ K}}(n) = -0.06688\log^{2}(n) + 2.18936\log(n) - 17.9151 \tag{35}$$

Similarly to AlAsSb, we introduce the temperature dependence of refractive index of InAsSb [6]: $(1/n_R)(\mathrm{d}n_R/\mathrm{d}T) = [1.2\times 10^{-4}x + 6.9\times 10^{-5}(1-x)]$ K^{-1}, where x is the As content.

To calculate the refractive index for α-Si, we recommend the following formula:

$$n_{R,\ \alpha\text{-Si}}(E) = 0.144 + \frac{3.308}{1 - 0.0437E^{2}} \tag{36}$$

which we derived from experimental data given in [45]. On the basis of [46] we assume $dn_R/dT = 2.2 \times 10^{-5}$ K^{-1} for this material. From [45] we also estimated the formula for absorption coefficient in α-Si:

$$\alpha_{\alpha\text{-Si}}(E) = 10^{2.506E + 0.2} \tag{37}$$

To calculate the n_R for SiO_2, the formula given in [47] can be used. Moreover, from [47] the temperature dependence of this parameter can be derived: $dn_R/dT = 1.1 \times 10^{-5}$ K^{-1}. Taking into consideration the results presented in [48], we formulated the following formula for absorption coefficient in SiO_2:

$$\alpha_{SiO_2}(\lambda) = 0.982\lambda - 3.542 \tag{38}$$

where λ is given in μm.

3. Results

As a verification of correctness of the set of material data and the formulas describing the relations of those data as functions of alloy composition, temperature and carrier concentration we compared the experimental and numerical results for the voltage-current characteristics and ambient temperature dependences of the threshold current (Fig. 1). Calculations have been carried out for the structure (Fig. 2) very similar to the currently most modern 2.6 μm GaInAsSb/GaSb VCSEL proposed in [4]. Its intentionally undoped active region is assumed to be composed of 10-nm $Ga_{0.50}In_{0.50}As_{0.185}Sb_{0.815}$ quantum wells separated by 8-nm GaSb barriers. The active region is embedded in $Al_{0.10}Ga_{0.90}As_{0.01}Sb_{0.99}$ waveguide and sandwiched by *p*- and *n*-type GaSb spacers. Above *p*-type spacer, the tunnel junction (TJ) composed of p^{++}-GaSb and n^{++}-$InAs_{0.91}Sb_{0.09}$ is located. To minimize the absorption loss, the TJ is situated

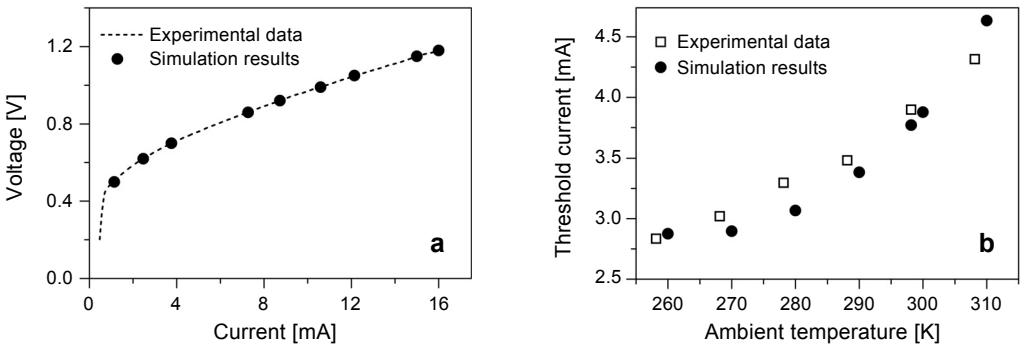

Fig. 1. Comparison between experimental and numerical results for the: voltage-current characteristics (**a**), and ambient temperature dependences of the threshold current (**b**).

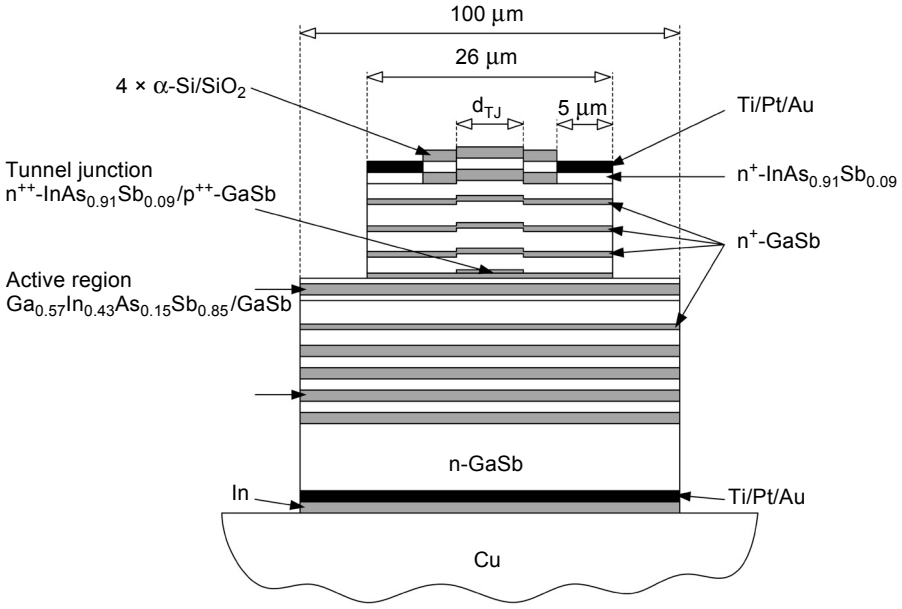

Fig. 2. The schematic structure of the antimonide-based VCSEL.

at the standing-wave node. Upper spacer is manufactured from *n*-GaSb. The 3-λ cavity with several n^+-GaSb current spreading layers situated in cavity nodes is terminated on both sides by distributed-Bragg-reflectors (DBRs): the 4-pair α-Si/SiO_2 top DBR and the 24-pair $AlAs_{0.08}Sb_{0.92}$/GaSb bottom *n*-type DBR. Bottom DBR diameter is assumed to be equal to 60 µm, whereas the upper DBR diameter is larger by 6 µm than TJ diameter. The top contact is produced in a form of a ring of 10 µm width. It is separated from the top spacer with the 200-nm thick highly-doped n^+-$InAs_{0.91}Sb_{0.09}$ contact layer. The whole bottom 60 µm diameter surface of the 500-µm *n*-type GaSb substrate is covered by the bottom contact.

As can be seen in Fig. 1**a**, there is a very good agreement between experimental data for the voltage-current characteristics and theoretical results obtained with the use of our model. From that we can conclude that the electrical parameters (electrical conductivities, mobilities, and free carrier concentrations) and the thermal conductivities have been correctly estimated. A slightly poorer agreement has been found for the ambient temperature dependences of the threshold current (Fig. 1**b**). However, the general trend, according to which the threshold current increases with the ambient temperature, is similar. The observed discrepancy can take its origin from the fact that in real structure quantum wells have slightly different material compositions and widths, whereas, in the simulation, they were identical to simplify the calculations. Moreover, we assumed that the carrier concentration is the same in every quantum well, which is not true in the real device. Both simplifications lead to broadening of the gain spectrum,

and therefore have an influence on the ambient temperature dependences of the threshold current. Nevertheless, the gain and optical parameters seem to have reasonable values to perform the simulation of a device based on the materials mentioned in this work.

4. Conclusions

In order to perform the comprehensive simulation of the operation of a semiconductor device, it is necessary to make use of the complex self-consistent numerical model which is composed of electrical, thermal, recombination and optical models. The most important feature of this approach is that it allows the integration of various physical phenomena taking place within a laser device and is crucial for its operation. Therefore, in calculations, it is necessary to include the material composition, temperature, carrier concentration, and wavelength dependences in electrical, thermal, recombination and optical modules. In this work, a complete set of material parameters which we obtained basing mostly on the experimental data has been presented. With the use of presented formulas, it is possible to calculate all the important parameters that are necessary to simulate the antimonide-based lasers emitting in the mid-infrared wavelength region. Results of such simulations can be found in our previous works [49, 50].

Acknowledgements – This work was supported by the Polish National Science Centre (DEC-2012/07/D/ST7/02581).

References

[1] PISKORSKI Ł., SARZAŁA R.P., *GaInNAs quantum-well vertical-cavity surface-emitting lasers emitting at 2.33 μm*, Bulletin of the Polish Academy of Sciences – Technical Sciences **61**(3), 2013, pp. 737–744.

[2] PISKORSKI Ł., SARZAŁA R.P., NAKWASKI W., *Investigation of temperature characteristics of modern InAsP/InGaAsP multi-quantum-well TJ-VCSELs for optical fibre communication*, Opto-Electronics Review **19**(3), 2011, pp. 320–326.

[3] KASHANI-SHIRAZI K., VIZBARAS K., BACHMANN A., ARAFIN S., AMANN M.-C., *Low-threshold strained quantum-well GaSb-based lasers emitting in the 2.5- to 2.7-μm wavelength range*, IEEE Photonics Technology Letters **21**(16), 2009, pp. 1106–1108

[4] ARAFIN S., BACHMANN A., KASHANI-SHIRAZI K., AMANN M.-C., *Continuous-wave electrically-pumped GaSb-based VCSELs at ~2.6 μm operating up to 50°C*, Proceedings of the 22nd Annual Meeting of the IEEE Photonics Society, October 4–8, 2009, Belek-Antalya, Turkey, pp. 837–838.

[5] CZICHOS H., SAITO T., SMITH L.M., *Springer Handbook of Materials Measurement Methods*, 1st Ed., Springer, Berlin, Heidelberg, 2006, p. 458.

[6] ADACHI S., *Properties of Group-IV, III-V and II-VI Semiconductors*, Wiley, Chichester, 2005.

[7] CHIU T.H., DITZENBERGER J.A., LUFTMAN H.S., TSANG W.T., HA N.T., *Te doping study in molecular beam epitaxial growth of GaSb using Sb_2Te_3*, Applied Physics Letters **56**(17), 1990, pp. 1688–1690.

[8] MIROWSKA A., ORŁOWSKI W., *Domieszkowanie monokryształów antymonku galu na typ przewodnictwa n oraz na typ p*, Materiały Elektroniczne **38**, 2010, pp. 17–32 (in Polish).

[9] CHEN J.F., CHO A.Y., *Characterization of Te-doped GaSb grown by molecular beam epitaxy using SnTe*, Journal of Applied Physics **70**(1), 1991, pp. 277–281.

[10] CHANG-EUN KIM, KUROSAKI K., MUTA H., OHISHI Y., YAMANAKA S., *Thermoelectric properties of Zn-doped GaSb*, Journal of Applied Physics **111**(4), 2012, article 043704.

[11] YANO M., SUZUKI Y., ISHII T., MATSUSHIMA Y., KIMATA M., *Molecular beam epitaxy of GaSb and $GaSb_xAs_{1-x}$*, Japanese Journal of Applied Physics **17**(12), 1978, pp. 2091–2096.

[12] SUBBANNA S., TUTTLE G., KROEMER H., *N-type doping of gallium antimonide and aluminum antimonide grown by molecular beam epitaxy using lead telluride as a tellurium dopant source*, Journal of Electronic Materials **17**(4), 1988, pp. 297–303.

[13] WANG C.A., SHIAU D.A., HUANG R.K., HARRIS C.T., CONNORS M.K., *Organometallic vapor phase epitaxy of n-GaSb and n-GaInAsSb for low resistance ohmic contacts*, Journal of Crystal Growth **261**(2–3), 2004, pp. 379–384.

[14] TURNER G.W., EGLASH S.J., STRAUSS A.J., *Molecular-beam epitaxy growth of high-mobility n-GaSb*, Journal of Vacuum Science and Technology B **11**(3), 1993, pp. 864–867.

[15] PINO R., KO Y., DUTTA P.S., *High-resistivity GaSb bulk crystals grown by the vertical bridgman method*, Journal of Electronic Materials **33**(9), 2004, pp. 1012–1015.

[16] JOHNSON G.R., CAVENETT B.C., KERR T.M., KIRBY P.B., WOOD C.E.C., *Optical, Hall and cyclotron resonance measurements of GaSb grown by molecular beam epitaxy*, Semiconductor Science and Technology **3**(12), 1988, pp. 1157–1165.

[17] STIRN R.J., BECKER W.M., *Galvanomagnetic effects in p-type AlSb*, Physical Review **148**(2), 1966, pp. 907–919.

[18] ADACHI S., *Handbook on Physical Properties of Semiconductors*, Vol. 2, Springer, Berlin, Heidelberg, 2004, p. 196.

[19] HARMAND J.C., KOHL A., JUHEL M., LE ROUX G., *Molecular beam epitaxy of AlGaAsSb system for 1.55 μm Bragg mirrors*, Journal of Crystal Growth **175/176**, 1997, pp. 372–376.

[20] MADELUNG O., RÖSSLER U, SCHULZ M., *Group IV Elements, IV-IV and III-V Compounds*, Springer, Berlin, 2002.

[21] WANG C.A., CHOI H.K., *OMVPE growth of GaInAsSb/AlGaAsSb for quantum-well diode lasers*, Journal of Electronic Materials **26**(10), 1997, pp. 1231–1236.

[22] BENNETT B.R., MOORE W.J., YANG M.J., SHANABROOK B.V., *Transport properties of Be- and Si-doped AlSb*, Journal of Applied Physics **87**(11), 2000, pp. 7876–7879.

[23] BARASKAR A., JAIN V., WISTEY M.A., SINGISETTI U., YONG-JU L. THIBEAULT B., GOSSARD A., RODWELL M.J.W., *High doping effects on in-situ Ohmic contacts to n-InAs*, Proceedings of the 22nd International Conference on Indium Phosphide and Related Materials, May 31–June 4, 2010, Kagawa, Japan.

[24] MURDIN B.N., LITVINENKO K., ALLAM J., PIDGEON C.R., BIRD M., MORRISON K., ZHANG T., CLOWES S.K., BRANFORD W.R., HARRIS J., COHEN L.F., *Temperature and doping dependence of spin relaxation in n-InAs*, Physical Review B **72**(8), 2005, article 085346.

[25] LI LI-GONG, LIU SHU-MAN, LUO SHUAI, YANG TAO, WANG LI-JUN, LIU FENG-QI, YE XIAO-LING, XU BO, WANG ZHAN-GUO, *Metalorganic chemical vapor deposition growth of InAs/GaSb superlattices on GaAs substrates and doping studies of p-GaSb and n-InAs*, Chinese Physics Letters **29**(7), 2012, article 076801.

[26] DIAMOND A.S., WEISS D. S., *Handbook of Imaging Materials*, 2nd Ed., Marcel Dekker, New York, Basel, 2002, p. 630.

[27] SHACKELFORD J.F., ALEXANDER W., *CRC Materials Science and Engineering Handbook*, 3rd Ed., CRC Press LLC, Boca Raton 2001, chap. 7.

[28] GARNACHE A., OUVRARD A., CERUTTI L., BARAT D., VICET A., GENTY F., ROUILLARD Y., ROMANINI D., CERDA-MENDEZ E.A., *2–2.7 μm single frequency tunable Sb-based lasers operating in CW at RT: microcavity and external cavity VCSELs, DFB*, Proceedings of SPIE **6184**, 2006, article 61840N.

[29] ANIKEEV S., DONETSKY D., BELENKY G., LURYI S., WANG C.A., BORREGO J.M., NICHOLS G., *Measurement of the Auger recombination rate in p-type 0.54 eV GaInAsSb by time-resolved photoluminescence*, Applied Physics Letters **83**(16), 2003, pp. 3317–3319.

[30] DONETSKY D., ANIKEEV S., GU N., BELENKY G., LURYI S., WANG C.A., SHIAU D.A., DASHIELL M., BEAUSANG J., NICHOLS G., *Analysis of recombination processes in 0.5–0.6 eV epitaxial GaInAsSb*

lattice-matched to GaSb, Proceedings of the American Institute of Physics **738**, June 14–16, 2004, Freiburg, Germany, pp. 320–328 (in Polish).

[31] GADEDJISSO-TOSSOU K.S., BELAHSENE S., MOHOU M.A., TOURNIÉ E., ROUILLARD Y., *Recombination channels in 2.4–3.2 μm GaInAsSb quantum-well lasers*, Semiconductor Science and Technology **28**(1), 2013, article 015015.

[32] PISKORSKI Ł., *Modelling of physical phenomena in the selected VCSEL structures emitting at the second telecommunication window wavelength*, PhD Thesis, Lodz University of Technology, Łódź, 2010 (in Polish).

[33] ADACHI S., *Properties of Semiconductor Alloys: Group-IV, III-V and II-VI Semiconductors*, Wiley, Chichester, 2009, pp. 63–75.

[34] CAHILL D.G., KATIYAR M., ABELSON J.R., *Thermal conductivity of a-Si:H thin films*, Physical Review B **50**(9), 1994, pp. 6077–6081.

[35] CAHILL D.G., *Thermal conductivity measurement from 30 to 750 K: the 3ω method*, Review of Scientific Instruments **61**(2), 1990, pp. 802–808.

[36] VURGAFTMAN I., MEYER J.R., RAM-MOHAN L.R., *Band parameters for III-V compound semiconductors and their alloys*, Journal of Applied Physics **89**(11), 2001, pp. 5815–5875.

[37] GLISSON T.H., HAUSER J.R., LITTLEJOHN M.A., WILLIAMS C.K., *Energy bandgap and lattice constant contours of III-V quaternary alloys*, Journal of Electronic Materials **7**(1), 1978, pp. 1–16.

[38] MUNOZ URIBE M., DE OLIVEIRA C.E.M., CLERICE J.H., MIRANDA R.S., ZAKIA M.B., DE CARVALHO M.M.G., PATEL N.B., *Measurement of refractive index of GaSb (1.8 to 2.56 μm) using a prism*, Electronics Letters **32**(3), 1996, pp. 262–264.

[39] ASPNES D.E., STUDNA A.A., *Dielectric functions and optical parameters of Si, Ge, GaP, GaAs, GaSb, InP, InAs, and InSb from 1.5 to 6.0 eV*, Physical Review B **27**(2), 1983, pp. 985–1009.

[40] PASKOV P.P., *Refractive indices of InSb, InAs, GaSb, $InAs_xSb_{1-x}$, and $In_{1-x}Ga_xSb$: effects of free carriers*, Journal of Applied Physics **81**(4), 1997, pp. 1890–1898.

[41] CHANDOLA A., PINO R., DUTTA P.S., *Below bandgap optical absorption in tellurium-doped GaSb*, Semiconductor Science and Technology **20**(8), 2005, pp. 886–893.

[42] CLUGSTON D.A., BASORE P.A., *Modelling free-carrier absorption in solar cells*, Progress in Photovoltaics: Research and Applications **5**(4), 1997, pp. 229–236.

[43] SANCHEZ D., *Nouveau système de confinement pour le VCSEL GaSb*, PhD Thesis, Université de Montpellier, Montpellier, 2012 (in French).

[44] ALIBERT C., SKOURI M., JOULLIE A., BENOUNA M., SADIQ S., *Refractive indices of AlSb and GaSb-lattice -matched $Al_xGa_{1-x}AsySb_{1-y}$ in the transparent wavelength region*, Journal of Applied Physics **69**(5), 1991, pp. 3208–3211.

[45] ARAFIN S., *Electrically-pumped gasb-based vertical-cavity surface-emitting lasers*, PhD Thesis, Technischen Universität München, Munich, 2011.

[46] DO N., KLEES L., LEUNG P.T., TONG F., LEUNG W.P., TAM A.C., *Temperature dependence of optical constants for amorphous silicon*, Applied Physics Letters **60**(18), 1992, pp. 2186–2188.

[47] MALITSON I. H., *Interspecimen comparison of the refractive index of fused silica*, Journal of the Optical Society of America **55**(10), 1965, pp. 1205–1209.

[48] KITAMURA R., PILON L., JONASZ M., *Optical constants of silica glass from extreme ultraviolet to far infrared at near room temperature*, Applied Optics **46**(33), 2007, 8118–8133.

[49] PISKORSKI Ł., WALCZAK J., DEMS M., BELING P., SARZAŁA R.P., *Modelowanie i optymalizacja antymonkowych laserów typu VCSEL*, Przegląd Elektrotechniczny **91**, 2015, pp. 150–153 (in Polish).

[50] PISKORSKI Ł., SARZAŁA R.P., WALCZAK J., DEMS M., BELING P., SOKÓŁ A.K., NAKWASKI W., *Transverse-mode selectivity in antimonide-based vertical-cavity surface-emitting lasers*, 17th International Conference on Transparent Optical Networks (ICTON), July 5–9, 2015, Budapest, Hungary.

Received November 7, 2015
in revised form December 9, 2015